Fundamental study of blue wavelength laser for welding low thickness dissimilar Cu and steel materials

Iqbal, N. & Sadeghian, A.

Published PDF deposited in Coventry University's Repository

Original citation:
Iqbal, N & Sadeghian, A 2023, 'Fundamental study of blue wavelength laser for welding low thickness dissimilar Cu and steel materials', Materials Today Communications, vol. 36, 106604.
https://dx.doi.org/10.1016/j.mtcomm.2023.106604

DOI 10.1016/j.mtcomm.2023.106604
ISSN 2352-4928

Publisher: Elsevier

This is an open access article under the CC BY license
(http://creativecommons.org/licenses/by/4.0/)

Materials Today Communications 36 (2023) 106604

Contents lists available at ScienceDirect

Materials Today Communications

journal homepage: www.elsevier.com/locate/mtcomm

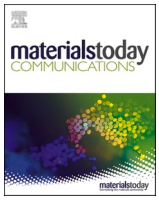

Fundamental study of blue wavelength laser for welding low thickness dissimilar Cu and steel materials

Naveed Iqbal [a,*], Amirhossein Sadeghian [b,*]

[a] ITP Aero, Dorey Way, Hucknall, Nottinghamshire NG15 6EU, UK
[b] Institute for Advanced Manufacturing and Engineering, Coventry University, CV6 5LZ, UK

ARTICLE INFO

Keywords:
Blue laser welding
Dissimilar materials
Copper
Steel
Microstructure
Microhardness

ABSTRACT

The present study reports on the application of blue wavelength (450 nm), continuous wave laser welding of Ni-coated copper to mild steel in lap joint configuration. The laser power was varied from 1 kW to 1.5 kW in incremental steps of 0.1 kW whilst the welding speed was kept constant at 6 m/min. Metallographic examination of the weld samples revealed that the weld penetration and width strongly correlated to the laser power, the characteristic of a stable welding process due to the high absorption of the blue wavelength laser. No substantial cracks or a large number of porosities were observed in the welds. The mechanical properties of the weld samples were characterized through tensile testing and microhardness measurements to establish the microstructure property relationship. The maximum tensile strength measured for specified weld geometries was 649 N with corresponding weld efficiency of 91%. The higher-strength welds showed a tensile fracture in the heat-affected zone (HAZ) of Cu, at the periphery of weld nuggets while lower-strength welds showed interfacial fracture due to the lack of fusion. In samples made with sufficient penetration the joint strength was controlled by the HAZ rather than the joint microstructure. A significant increase in the microhardness was measured inside the weld nugget compared to the parent materials, attributed to the formation of Cu-Fe composite microstructure owing to the inter-mixing of Cu and Fe during welding. The highest microhardness was observed in the HAZ of the mild steel due to martensitic microstructure formation in this region.

1. Introduction

Joining dissimilar materials is a great technological and engineering challenge [1]. The need for joints between dissimilar materials often arises in industrial applications of complex functionality. During recent years the dissimilar joining of highly conductive materials such as copper, aluminium and steel with varying sheet thickness combinations, have gained particular interest due to their applications in emerging energy storage industries including the electronic industry and EV battery manufacturing [2,3]. For example, battery systems operate with electricity stored in large battery assemblies with up to several thousand single battery cells connected using steel cell tabs to copper bus-bar interconnect joints [4,5]. Every single joint influences the functionality and efficiency of the whole battery system. Functional reliability requires a large weld interface area to reduce electrical contact resistance, decrease current density and increase mechanical strength [6].

A variety of joining techniques have previously been explored to join dissimilar materials including ultrasonic welding, resistance spot welding, pulsed arc welding and laser welding [7]. Laser welding is of interest due to its high energy density, non-contact nature, and ease to adjust to a wide range of designs and constrained geometries which makes it a time-efficient manufacturing process [8,9]. Laser welding is also known as a low-distortion and low-deformation joining process [10]. However, laser welding has its own challenges, especially when applied to highly reflective materials like copper, aluminium etc. The commonly used infrared (IR) wavelength (wavelength: ~1064 nm) lasers, exhibit low absorption for these materials thereby limiting the process efficiency and reproducibility [11,12] while in today's market environment, there is a continuing demand towards a reduction of product development times. A possible approach to overcome this challenge is the use of high absorptive blue wavelength (wavelength: ~450 nm) laser systems [13]. The variation in laser absorptivity with wavelength for various materials is reported in the literature and the absorptivity of blue wavelength is 13 times higher than IR wavelength for solid copper metal (65% for blue wavelength compared to 5% for IR) [14,15]. This reduces the amount of energy required for welding,

* Corresponding authors.
E-mail addresses: naveed.iqbal@itpaero.com (N. Iqbal), sadeghiana@uni.coventry.ac.uk (A. Sadeghian).

https://doi.org/10.1016/j.mtcomm.2023.106604
Received 17 May 2023; Received in revised form 15 June 2023; Accepted 3 July 2023
Available online 5 July 2023
2352-4928/© 2023 The Author(s). Published by Elsevier Ltd. This is an open access article under the CC BY license (http://creativecommons.org/licenses/by/4.0/).

Table 1
Physical and mechanical properties of C110 copper and DC01 mild steel.

	C110	DC01
Melting point [°C]	1083	1515
Density [g/cm^3]	8.94	7.9
Electrical resistivity [μΩ.m]	0.017	0.097
Thermal conductivity [W/m.K]	399	57.8
Young's modulus [GPa]	117	200–215
Tensile strength [MPa]	200–360	270–390
Thermal expansion [K^{-1}]	17.3×10^{-6}	12.1×10^{-6}

Table 2
Optics specifications of the laser system.

Laser System	LDMblue1500-60
Emission mode	Continuous wave
Wavelength [nm]	450
Laser Power [W]	1500
Focal Length [mm]	100
Numerical Aperture	0.22
Fibre Diameter [μm]	600
Beam Quality [mm.mrad]	60

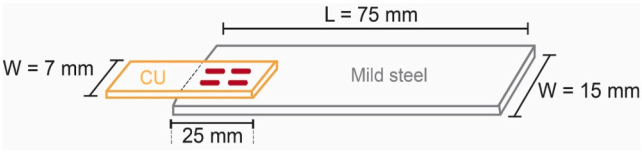

Fig. 1. Schematics of the overlap joint configuration of the dissimilar joint between Ni-coated Cu with mild steel (four weld lines in the overlap region are visible as red lines).

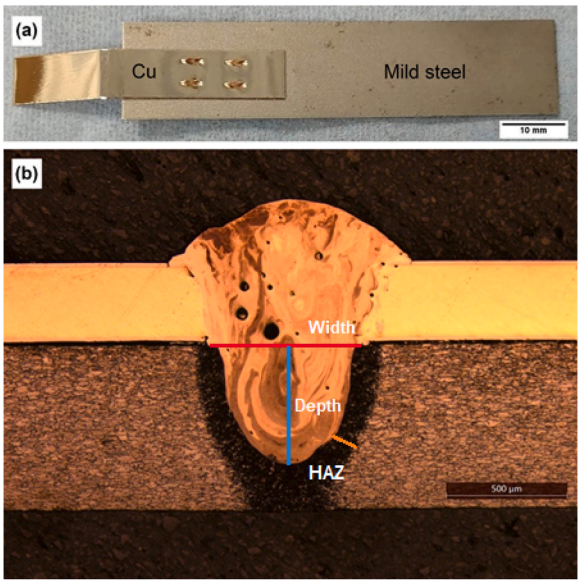

Fig. 2. (a) Weld photograph of blue laser weld sample, and (b) Optical micrograph of the weld sample produced using laser power 1.5 kW and welding speed 6 m/min.

provides better control of the processing window for highly-reflective materials and produces welds with improved strength and reproducibility [16].

Up until a few years ago, the maximum output power of blue laser sources in continuous wave (CW) mode was limited to several hundred watts [17]. Recent developments meanwhile have made high output power of 1.5 kW possible, making this type of laser more suitable for industrial applications [18]. Zediker et al. [19] evaluated the applicability of 500 W and 1000 W blue laser systems for different copper joint configurations including foil, thin sheets, and dissimilar joints of copper with steel and aluminium. Britten et al. [20] used a high-power blue laser source for cylindrical and pouch cell battery joining. High-speed videography showed a homogenous weld bead without spatters due to a high absorption level of blue wavelength. Das et al. [21] studied blue laser welding of stainless-steel micro-foils. A fast welding process with no visible cracks and little porosities in the weld region was achieved. Hummel et al. [22] used in situ X-ray tomography to compare laser welding of Cu-ETP and CuSn6 sheets with laser sources of 515 nm and 1030 nm wavelengths. A steadier process was observed for 515 nm wavelength compared to 1030 nm. Punzel et al. [23] compared three different technologies of infrared welding with beam oscillation, adjustable ring mode (ARM) fibre laser, and welding with a visible wavelength (wavelength: ~ 515 nm) for joining copper sheets. They found that although a stable process window for copper-to-copper welding could be achieved with all three approaches, welds generated by green wavelength had the highest stability and the least requirement for laser power. Blue laser lap welding of thin copper to aluminium was studied by Zapico et al. [24]. The process window for the formation of good joints without visible defects was reported to be larger than infrared laser.

According to published literature, the blue laser has the advantages of a large process window and good process stability. As a result, blue laser technology and its applications are developing fast, but the number of scientific studies investigating the application of blue wavelength in laser welding of dissimilar materials is limited. In the present study, a recently developed high-power blue laser source (1.5 kW) is used for welding Ni-coated copper and mild steel combination which is common in the EV industry. The weld microstructure was studied, and the mechanical properties of welds were characterized through microhardness measurements and tensile tests.

2. Materials and method

The materials used in this study were 0.3 mm thick high-purity C110 copper (99.95%) and 0.7 mm thick mild steel (DC01). A nickel coating with a thickness of 3 μm was implemented on copper. Copper was placed at the top of the mild steel, in an overlap joint configuration. The coupon size for the upper sheet (C110) was 7 mm × 50 mm while the bottom sheet (DC01) had a dimension of 15 mm × 75 mm. The physical and mechanical properties of the materials are presented in Table 1.

Prior to welding, all the coupons were degreased with acetone to remove any surface contamination. Small segmented welds were selected due to the requirements in EV battery manufacturing where cell tabs are quite small requiring small welds for electrical connections. The schematics of the overlap weld configuration and weld lines are shown in Fig. 1. The laser welding was performed using a continuous wave (CW) blue laser (LDMblue1500–60, Laserline), with a maximum peak power of 1.5 kW and a wavelength of 450 nm. Laser optics specifications are presented in Table 2. The optics generated a focused beam diameter of 600 μm with the focal position set on the workpiece surface. Argon was used as a shielding gas with a flow rate of 5 l/min. The process parameters for visually acceptable welds included a fixed welding speed of 6 m/min, whilst the laser power varied from 1 kW to 1.5 kW in incremental steps of 0.1 kW.

The cross-sections from the weld samples were mechanically ground using standard metallographic preparation techniques, including final polishing using a suspension of 1 μm colloidal silica. The samples were further etched using 10% Nital solution. The weld microstructure was analyzed using a Leica DFC295 optical microscopy, and a Hitachi TM4000 scanning electron microscopy (SEM) equipped with energy-dispersive X-ray spectroscopy (EDS). To evaluate the mechanical strength of the weld samples, tensile tests were performed. The

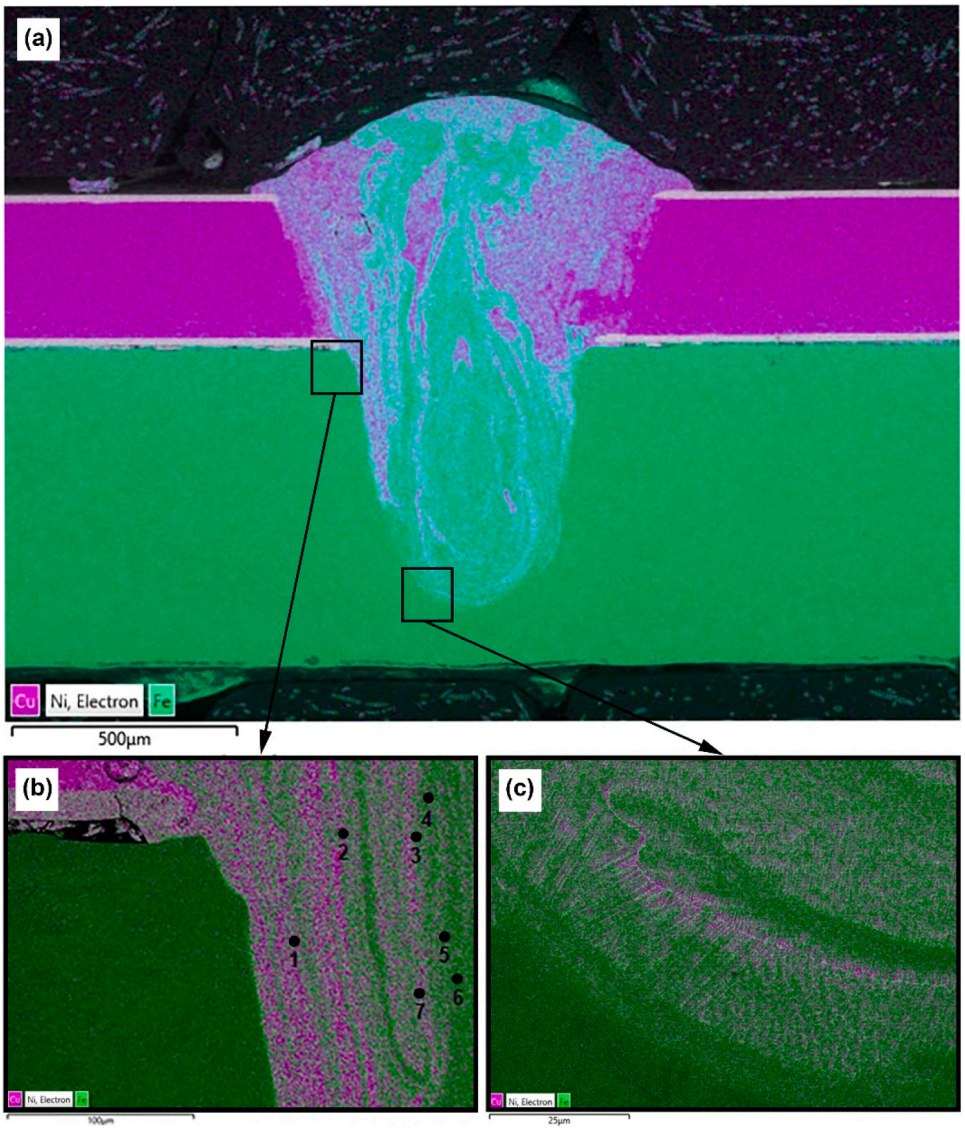

Fig. 3. (a) Elemental distribution in the weld nugget. (b), and (c) higher magnification images of specified locations.

horizontal line scans across the weld nugget and the vertical line scans measuring microhardness from top to bottom of polished samples using a test load of 100 gf and a dwell time of 15 s were performed.

3. Results and discussion

The top view of the weld sample produced using a laser power of 1.5 kW and a welding speed of 6 m/min is shown in Fig. 2(a). While melt ejections can happen in the laser welding of copper especially in high welding powers or low welding velocities [24], visual inspection of the weld surface indicates no presence of melt ejections. The weld optical micrograph is presented in Fig. 2(b). The interface width, penetration depth and heat-affected zone (HAZ) are indicated with red, blue and orange line, respectively. Despite the high welding speed and also high thermal conductivity of copper, a significant weld penetration is observed in the optical micrograph. This is encouraging since the higher welding speed is usually associated with a higher production rate in the manufacturing environment.

The weld microstructure is composed of a typical weld nugget, surrounded by the HAZ in copper, as well as in mild steel. No substantial cracks appeared in the weld zone. However, a few porosities with varied sizes can be seen inside the weld nugget. As the pores are spherical they are most likely formed due to gas entrapment. To make a careful study of the Cu-steel interface, higher magnification EDS images were taken. These images are shown in Fig. 3. A significant Fe element infiltrated into the molten copper to form a Cu-Fe solid solution resulting in a composite microstructure as evidenced by the EDS images, shown in Fig. 3(a). The EDS scanning data close to the weld interface as shown in Fig. 3(b), is listed in Table 3. It can be seen that the content of Fe and Cu elements inside the weld nugget varied greatly. Fig. 3(c) shows the weld microstructure near the mild steel interface. Fine ε-Cu and α-Fe phases

Table 3
EDS point analysis elemental data from Fig. 3(b).

Spectrum	Cu		Fe		Ni	
	wt%	at%	wt%	at%	wt%	at%
1	78.17	76.02	18.58	20.56	3.25	3.42
2	73.79	71.37	22.12	24.42	4.02	4.21
3	81.73	79.85	14.98	16.66	3.30	3.49
4	51.46	48.39	42.41	45.37	6.13	6.24
5	84.58	82.29	13.15	14.67	2.27	2.41
6	43.41	40.35	53.21	56.26	3.37	3.39
7	62.55	59.58	34.17	37.03	3.27	3.38

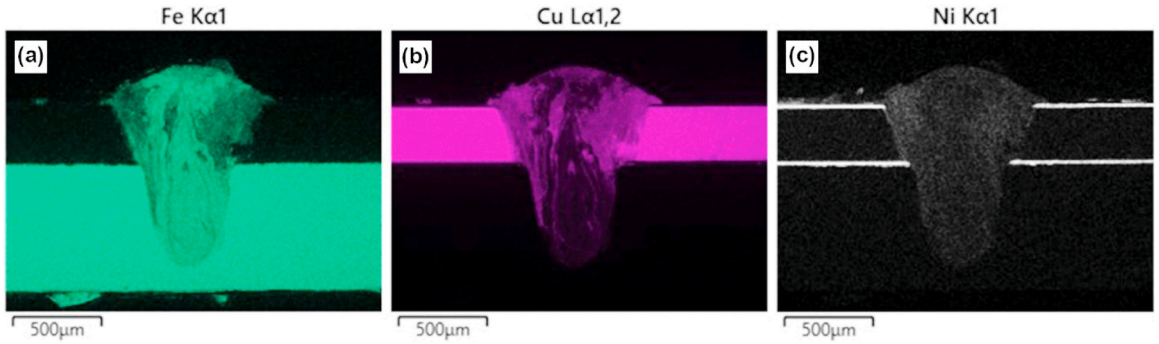

Fig. 4. EDS elemental maps showing (a) Fe and (b) Cu distribution inside the weld nugget. (c) Melting of Ni coating at the weld interface and its distribution.

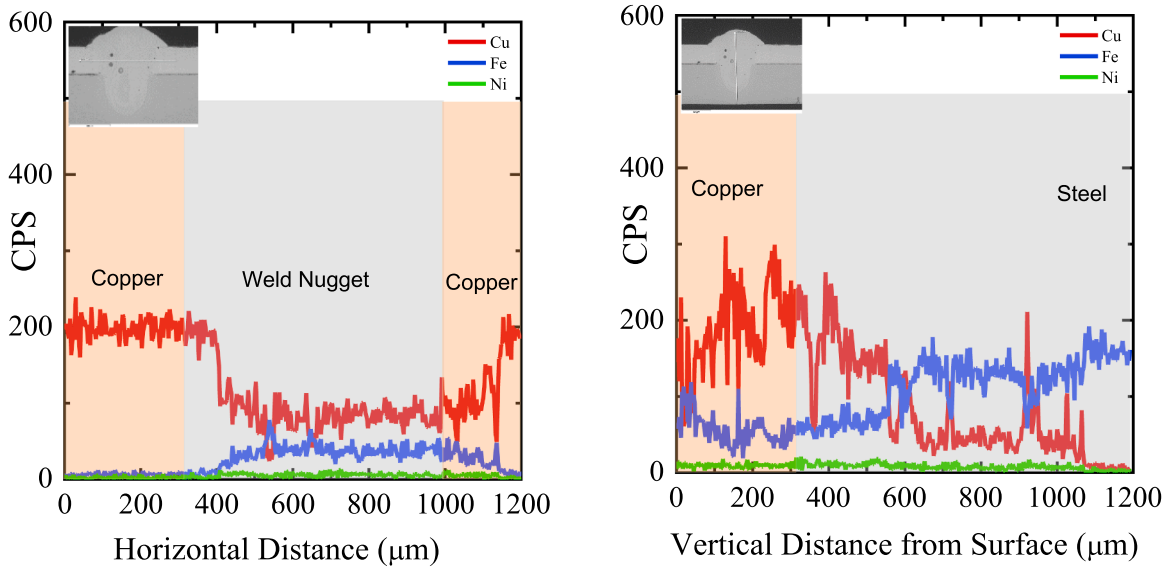

Fig. 5. The EDS line scans showing elemental distribution (a) Horizontal line scan in the mid thickness of Cu, across the weld nugget and (b) vertical line scan in the middle of the weld nugget.

are dominant in this region. No intermetallic (IMC) layer was observed at the weld interface between the mild steel and the weld nugget. The binary phase diagram of Cu-Fe also corroborate that no IMC is forms between Cu and Fe [25].

Fig. 4 further illustrates the elemental distribution maps with obvious macro segregation inside the weld nugget. The heterogeneity of Cu-Fe weld microstructure is previously reported in the literature [26]. Cu and Fe are reported to be immiscible in the liquid phase and undergo primary and secondary liquid separation due to the high cooling rate during laser welding, producing an inhomogeneous solution [27]. The macro segregations can greatly influence the physical properties such as elastic modulus and shrinkage at different locations of the weld nugget thereby resulting in sensitivity to cracks and poor mechanical properties [28]. Furthermore, the nickel coating on Cu is completely dissolved at the weld interface, while it remains visible outside the weld region. The horizontal and vertical line scans illustrating the elemental distribution along the weld width as well as weld depth are shown in Fig. 5. The results show that the elemental distribution is more uniform in the horizontal direction, compared to the vertical direction of the weld nugget potentially due to higher thermal gradients in the depth direction during welding. The Marangoni effect and the lower density led to the Fe elements moving towards the upper part of the weld. The results also support the potential formation of Fe-Cu solid solution with spatial elemental fluctuations as observed in the EDS point analysis presented in Table 3. The Ni content is almost evenly distributed in the weld region. The presence of Ni helps create a solid solution with Cu.

The microstructural transition in the HAZ of steel is further illustrated in Fig. 6. Fig. 6(a) and Fig. 6(b), exhibit the formation of a narrow band (100 μm wide) of martensitic microstructure in the proximity of the weld nugget due to a higher cooling rate in this region. The width of this martensitic band is significantly less compared to the previously reported 250 μm width when an infrared laser was used for the welding of the same materials [29]. Contrary to the typical keyhole formation during welding with infrared laser, blue wavelength laser interacts with Cu and steel to form a conduction mode molten pool, with reduced substrate temperature, resulting in reduced HAZ and potential metallurgical defects. The parent steel microstructure is shown in Fig. 6(d) indicating single-phase ferrite structure. A gradual microstructural transition from martensitic to parent material ferrite grains is illustrated in Fig. 6(c). It can be seen that the grains structure in the HAZ has been altered by the martensitic transformation, while the nucleation of martensitic grains at the grain boundaries of parent material away from HAZ is also evident.

Since laser power is the only variable welding parameter reported in this study while the welding speed remained unchanged, a change in laser power also corresponds to a change in total energy input into the weld metal. Evolution of weld nuggets at a constant welding speed of 6 m/min, but varied laser powers from 1.5 kW to 1.0 kW in incremental steps of 0.1 kW is shown in Fig. 7. It can be seen that the weld penetration depth and interface width decreases gradually with the decrease in laser power while the depth of penetration was more sensitive to the variation in laser power than interface width. When the laser power is

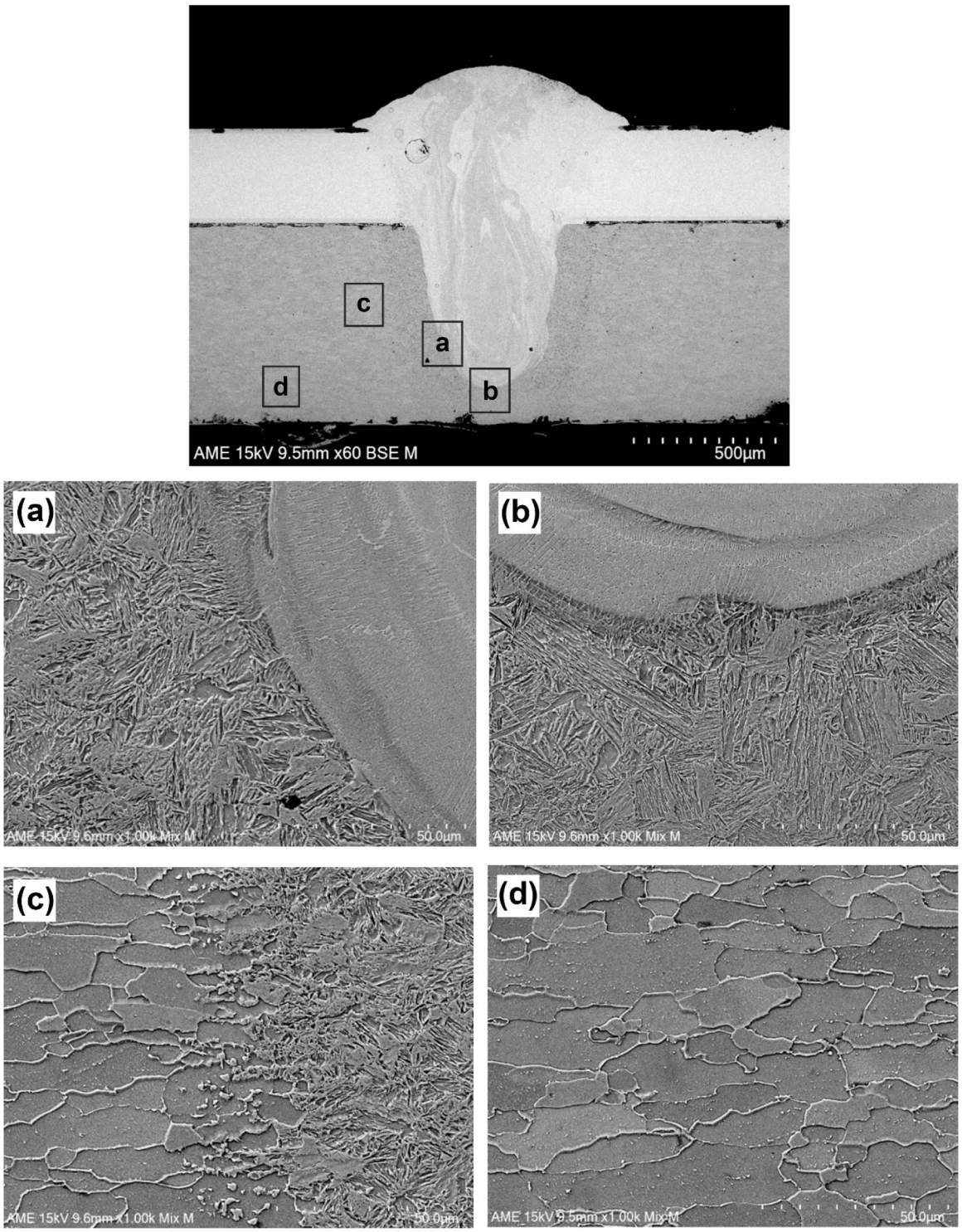

Fig. 6. The weld microstructure in different regions of the HAZ of DC01 steel. (a) and (b) martensitic structure of the HAZ in steel (c) the transition zone from martensitic HAZ to ferrite grains (d) the microstructure of parent steel showing ferrite structure.

1 kW, very little penetration is observed due to low laser-material interaction time leading to insufficient energy input per unit area that was not enough to overcome the high thermal conductivity of copper. The 1 kW weld failed at the interface during subsequent tensile testing. The comparison of EDS images also illustrates that the infiltration rate of Fe element into copper decreases at lower laser power potentially due to the reduced size of the molten pool and temperature gradients inside the molten pool.

Fig. 8(a) exhibits the variation in microhardness indent size in copper sheet close to the weld interface for laser power 1.5 kW. It can be seen that the indent size in the HAZ of copper is significantly larger compared to that in the weld nugget where Fe has infiltrated into copper. The softening of HAZ is expected due to grain coarsening in copper and is the region where tensile failure occurs in samples during testing as shown in Fig. 9. At the lowest laser power of 1.0 kW, the tearing does not happen at the top sheet and the weld failed at the interface potentially due to stronger HAZ in the Cu and reduced weld width and penetration depth. Fig. 8(b) further compares the micro-hardness indent size in

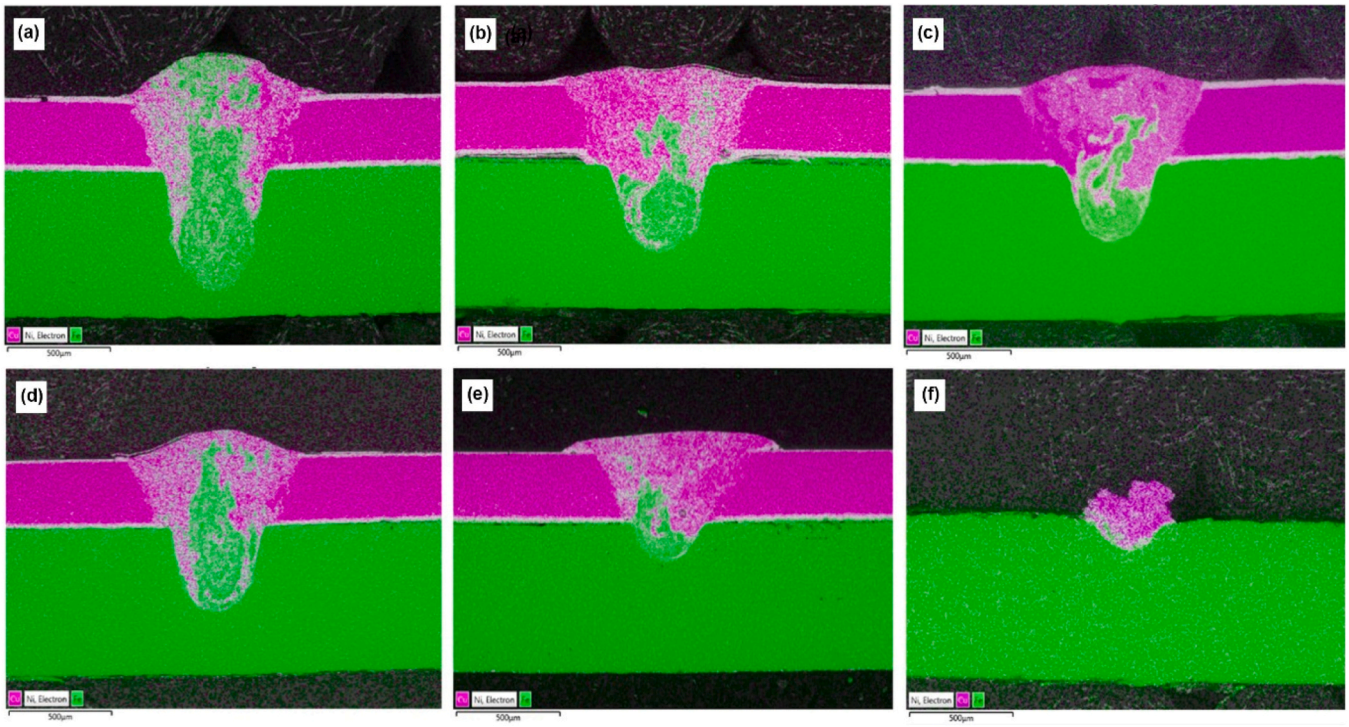

Fig. 7. (a-f) EDS Images showing weld penetration and elemental distribution inside welds, produced for varying laser power from 1.5 kW to 1.0 kW, using incremental steps of 0.1 kW. (f) Shows the weld fractured at the weld interface.

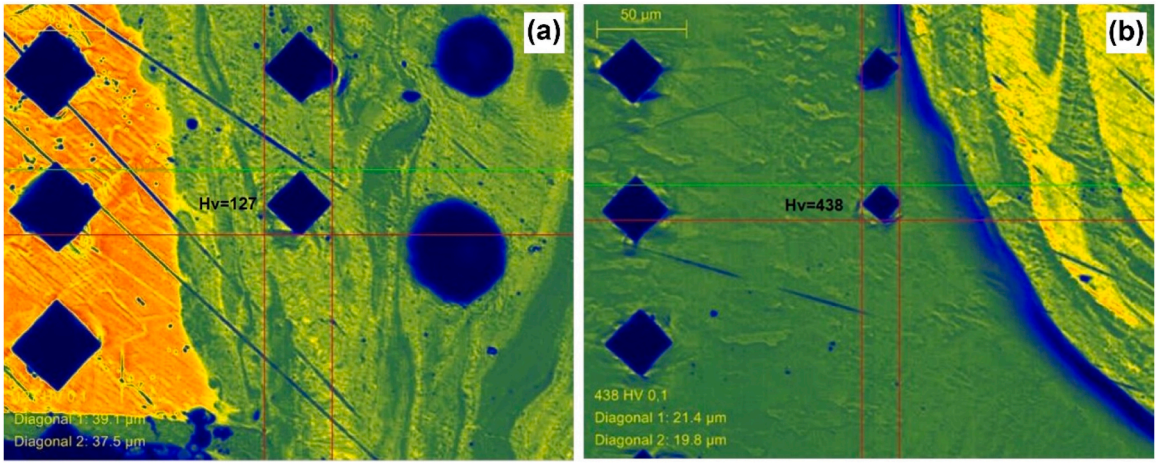

Fig. 8. (a) The change in microhardness indent size from HAZ of Cu to the weld nugget where Fe has infiltrated and (b) microhardness indent size variation from parent substrate DC01 steel to the HAZ where ferrite transformation to martensitic microstructure is observed.

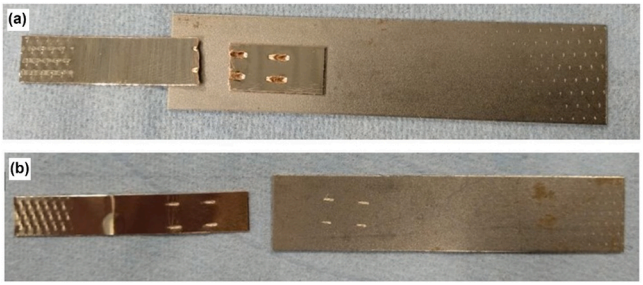

Fig. 9. The photographs of weld samples after tensile testing. (a) Laser power of 1.5 kW and failed at the HAZ of Cu. (b) Laser power of 1.0 kW and failed at the weld interface.

parent steel to that of the HAZ. A small indent size in the HAZ of steel is due to the higher hardness of the brittle martensitic phase reported earlier in microstructural investigation compared to ferrite structure.

Fig. 10 shows the vertical line scans for micro-hardness variation across the joint line. By moving from the copper sheet toward mild steel in the weld nugget region the microhardness increased due to more Fe element entering the weld creating Cu-Fe solid solution. Columns C_0 and C_6 exhibit the micro-hardness transition from HAZ of copper to parent steel. Again, low hardness in the HAZ of copper confirms the material softening owing to grain growth. However, the remaining columns exhibit regions of variable hardness with significant fluctuation, especially at the lower part of the weld nugget. The data is in good agreement with the results of microstructure characterisations showing regions of macro segregation. The highest hardness inside the weld nugget has a value of Hv= 430, quite close to the previously reported hardness data

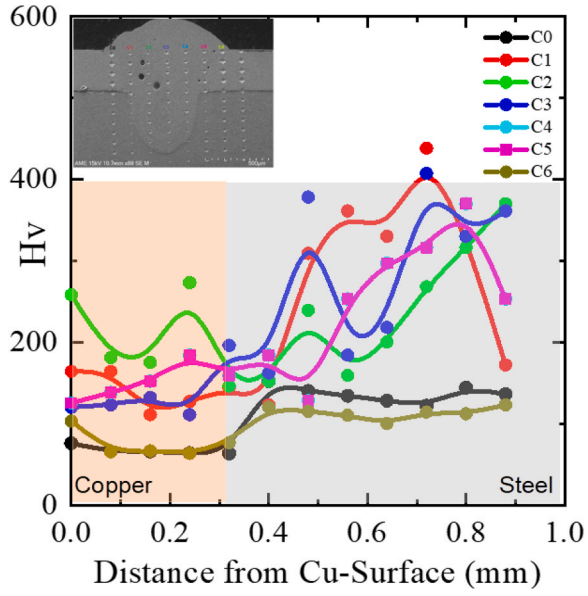

Fig. 10. The microhardness, vertical line scans in the weld sample produced for laser power 1.5 kW.

for Fe-Cu composite materials [30].

The variation in weld width, penetration depth and HAZ with the laser power is compared in Fig. 11(a). The results indicate that for the range of laser power used in this study, weld width is always higher than the penetration depth, a clear illustration of conduction mode welding which makes the process well-suited for joining low-thickness materials. However, it can be seen that the penetration depth gradually approaches the weld width with the increase in laser power. Furthermore, an increase in laser power can potentially result in transition welds that typically have a width-to-depth ratio of unity, with a temperature rise above the vaporization temperature similar to that reported previously [31]. The width of HAZ in steel is also observed to increase slowly with increasing heat input at higher laser powers.

The maximum force required to break the weld is used to compare the joint strength. Fig. 11(b), exhibits the tensile strength variation with laser power and compares it with that of the parent Cu sheet. The results indicate that the peak load for the 1.2 kW laser power and above does not significantly fluctuate before failure, meaning for the laser power of 1.2 kW and above the peak load plateaus, with an upper limit of 649 N. As mentioned earlier, the majority of the weld samples failed in the HAZ, thus, this observed peak load plateau can be largely attributable to the little changes in HAZ with further increase in laser power beyond 1.2 kW. The highest weld efficiency of 91% was calculated when compared to parent Cu. Only one weld showed an interfacial fracture, produced with the laser power of 1.0 kW, which had the smallest interface width and insufficient penetration. Due to insufficient penetration a weak joint was formed resulting in low maximum load.

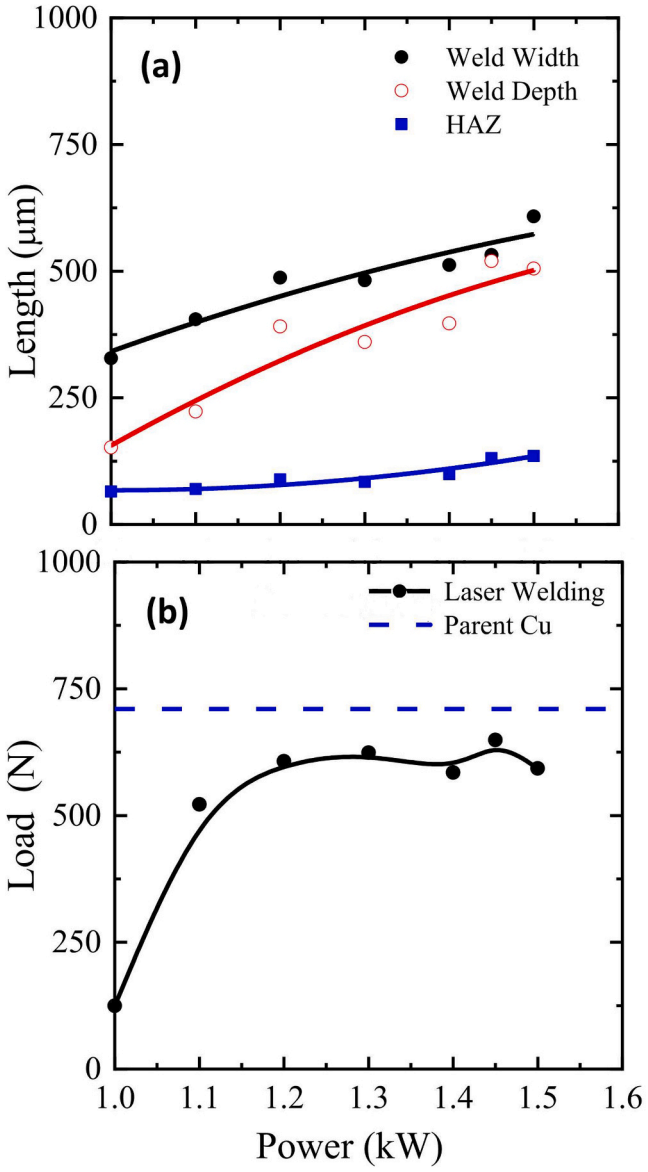

Fig. 11. (a) The variation in weld penetration, the width of weld interface and HAZ vs laser (b) The tensile strength of weld samples vs laser power. The same horizontal scale applies to both figures.

4. Conclusions

A feasibility study was carried out for the blue wavelength laser (wavelength: 450 nm), to weld dissimilar Ni-coated Cu and mild steel. Based on the process parameter development and the microstructure property relationship, the following conclusions can be drawn:

1. Low-thickness dissimilar materials (0.3 mm Ni-coated Cu and 0.7 mm mild steel) can be successfully welded by a blue wavelength laser system using a power range between 1.2 kW and 1.5 kW and a welding speed of 6 m/min.
2. The weld microstructure is composed of Cu-rich ε and Fe-rich α phases. Macro segregation of Cu and Fe inside the weld nugget is quite obvious and results in irregular microhardness variation inside the nugget.
3. The majority of the higher strength welds showed tensile failure mode in HAZ of Cu, indicating welds were sufficiently strong. The peak breaking load during tensile tests in samples with sufficient penetration depth was controlled by the width of the HAZ in Cu rather than the microstructure of the weld.
4. The peak load plateaus at laser powers above 1.1 kW. Therefore, laser welding can be achieved in conduction mode, at lower laser power and without transition to the keyhole mode.

Declaration of Competing Interest

The authors declare that they have no known competing financial interests or personal relationships that could have appeared to influence the work reported in this paper.

Data Availability

Data will be made available on request.

References

[1] S. Katayama, Laser welding of aluminium alloys and dissimilar metals, Weld. Int. 18 (8) (2004) 618–625.
[2] Mys, I. and M. Schmidt, *Chapter 8* - Laser Microspot Welding in Electronics Production☆, in *Advances in Laser Materials Processing* (*Second Edition*), J. Lawrence, Editor. 2018, Woodhead Publishing. p. 185–202.
[3] M.F.R. Zwicker, et al., Automotive battery pack manufacturing–a review of battery to tab joining, J. Adv. Join. Process. 1 (2020), 100017.
[4] M.J. Brand, et al., Welding techniques for battery cells and resulting electrical contact resistances, J. Energy Storage 1 (2015) 7–14.
[5] A. Das, et al., Joining technologies for automotive battery systems manufacturing, World Electr. Veh. J. 9 (2) (2018) 22.
[6] A. Sadeghian, N. Iqbal, A review on dissimilar laser welding of steel-copper, steel-aluminum, aluminum-copper, and steel-nickel for electric vehicle battery manufacturing, Opt. Laser Technol. 146 (2022), 107595.
[7] K. Martinsen, S.J. Hu, B.E. Carlson, Joining of dissimilar materials, CIRP Ann. 64 (2) (2015) 679–699.
[8] M. Jiang, et al., Enhanced penetration depth during reduced pressure keyhole-mode laser welding, Weld. J. 99 (2020) 110–124.
[9] Z. Tang, et al., Blue laser welding of laminated electrical steels: dynamic process, weld bead characteristics, mechanical and magnetic properties, J. Mater. Process. Technol. (2023), 117859.
[10] M. Jiang, et al., Mitigation of porosity defects in fiber laser welding under low vacuum, J. Mater. Process. Technol. 276 (2020), 116385.
[11] T.A. Mai, A.C. Spowage, Characterisation of dissimilar joints in laser welding of steel–kovar, copper–steel and copper–aluminium, Mater. Sci. Eng.: A 374 (1–2) (2004) 224–233.
[12] W.M. Steen, J. Mazumder, Laser Material Processing, Springer Science & Business Media, 2010.
[13] J. Zhou, et al., Comparison study of 6082 Al alloy laser welding using 455 nm blue laser and 1080 nm near-infrared laser, Optik 272 (2023), 170224.
[14] J.P. Davim, Nontraditional machining processes, Manuf. Process Sel. Handb. (2013) 205–226.
[15] R. Indhu, et al., Overview of laser absorptivity measurement techniques for material processing, Lasers Manuf. Mater. Process. 5 (4) (2018) 458–481.
[16] S. Dhara, et al., Utilising blue laser over infrared laser to enhance control of penetration depth and weld strength for producing electric vehicle battery interconnects, J. Mater. Process. Technol. 317 (2023), 117989.
[17] S. Engler, R. Ramsayer, R. Poprawe, Process studies on laser welding of copper with brilliant green and infrared lasers, Phys. Procedia 12 (2011) 339–346.
[18] M. Baumann, et al., 4XX nm diode-laser beyond 2 kW of output power, SPIE, 2022.
[19] M.S. Zediker, et al., Laser welding components for electric vehicles with a high-power blue laser system, J. Laser Appl. 32 (2) (2020), 022038.
[20] S.W. Britten, et al., Blue high-power laser sources for processing solutions in e-mobility and beyond, Procedia CIRP 94 (2020) 592–595.
[21] A. Das, et al., Blue laser welding of multi-layered AISI 316L stainless steel micro-foils, Opt. Laser Technol. 132 (2020), 106498.
[22] M. Hummel, et al., In situ X-ray tomography investigations on laser welding of copper with 515 and 1030 nm laser beam sources, J. Manuf. Process. 67 (2021) 170–176.
[23] E. Punzel, et al., Comparison of different system technologies for continuous-wave laser beam welding of copper, Procedia CIRP 94 (2020) 587–591.
[24] E. Perez Zapico, et al., Influence of process parameters in blue laser welding of copper and aluminum thin sheets, J. Laser Appl. 34 (4) (2022), 042039.
[25] H. Okamoto, Supplemental literature review of binary phase diagrams: Au-Dy, Au-Sc, Au-Yb, C-Hf, C-Ta, Cu-Fe, Dy-Mn, Er-Mn, Ho-Mn, Mn-Tb, Mn-Tm, and Sb-Sn, J. Phase Equilibria Diffus. 38 (2) (2017) 160.
[26] F. Yan, et al., Effects of beam oscillation on microstructural characteristics and mechanical properties in laser welded steel-copper joints, Opt. Laser Technol. 148 (2022), 107739.
[27] S. Chen, et al., Microstructural characteristics of a stainless steel/copper dissimilar joint made by laser welding, Metall. Mater. Trans. A 44 (8) (2013) 3690–3696.
[28] T. Michler, et al., Influence of macro segregation on hydrogen environment embrittlement of SUS 316L stainless steel, Int. J. Hydrog. Energy 34 (7) (2009) 3201–3209.
[29] Iqbal, N., et al. Parametric Study of Pulse Arc Welding (PAW) and Laser Beam Welding (LBW) Techniques for Electrical Vehicle Battery Cells. in Materials Science Forum. 2021. Trans Tech Publ.
[30] L. He, E. Ma, Processing and microhardness of bulk Cu-Fe nanocomposites, Nanostruct. Mater. 7 (3) (1996) 327–339.
[31] W. Ke, et al., Heat transfer and melt flow of keyhole, transition and conduction modes in laser beam oscillating welding, Int. J. Heat. Mass Transf. 203 (2023), 123821.